How to cite: Angew. Chem. Int. Ed. 2023, e202317345
doi.org/10.1002/anie.202317345

Nanoclusters

Modulation of Singlet-Triplet Gap in Atomically Precise Silver Cluster-Assembled Material

Priyanka Chandrashekar, Gopa Sardar, Turbasu Sengupta, Arthur C. Reber, Pradip Kumar Mondal, Dinesh Kabra, Shiv N. Khanna, Pravas Deria,* and Sukhendu Mandal**

Dedicated to Professor C. N. R. Rao on the occasion of his 90th birthday

Abstract: Silver cluster-based solids have garnered considerable attention owing to their tunable luminescence behavior. While surface modification has enabled the construction of stable silver clusters, controlling interactions among clusters at the molecular level has been challenging due to their tendency to aggregate. Judicious choice of stabilizing ligands becomes pivotal in crafting a desired assembly. However, detailed photophysical behavior as a function of their cluster packing remained unexplored. Here, we modulate the packing pattern of Ag_{12} clusters by varying the nitrogen-based ligand. CAM-1 formed through coordination of the tritopic linker molecule and NC-1 with monodentate pyridine ligand; established via non-covalent interactions. Both the assemblies show ligand-to-metal-metal charge transfer (LMMCT) based cluster-centered emission band(s). Temperature-dependent photoluminescence spectra exhibit blue shifts at higher temperatures, which is attributed to the extent of the thermal reverse population of the S_1 state from the closely spaced T_1 state. The difference in the energy gap (ΔE_{ST}) dictated by their assemblies played a pivotal role in the way that Ag_{12} cluster assembly in CAM-1 manifests a wider ΔE_{ST} and thus requires higher temperatures for reverse intersystem crossing (RISC) than assembly of NC-1. Such assembly-defined photoluminescence properties underscore the potential toolkit to design new cluster- assemblies with tailored optoelectronic properties.

Introduction

Synthesis of hierarchical molecular architectures constructed from atomically precise clusters as secondary building units (SBU) is one of the propitious directions in cluster research.[1] These cluster-assembled materials (CAMs) are unique in structure and can lead to tunable properties as a function of their inter-cluster and intra-cluster length scales.[2] Therefore, the physical properties of these CAMs can be defined in terms of the molecular structure (size and composition) of the SBU and the interconnecting linkers. Among the chemically robust molecular clusters that are suitable to serve as SBU, coinage metal-based systems have gained much attention.[3] Silver clusters are particularly intriguing due to their chemical activity (with their low redox potential) and their low, yet tuneable luminescent efficiency in ambient conditions.[4] Such tunability may be achieved through the CAM formation that also provides structural stability and defines optoelectronic properties and their photophysical behavior.[5]

Ligand-stabilized silver nanoclusters (Ag^I-NCs) give rise to a wide range of photoluminescence (PL) involving LMMCT, ligand-based n–π* and/or π–π* transitions, or inter-ligand trans-metallic charge transfer (ITCT)[6] mixed with cluster centered triplet excited state.[5a] Nevertheless, the cluster-centered emission—involving a triplet excited state—manifests spectral envelope and related photophysical properties that commonly display temperature-dependent behavior.[7] In this work, we have synthesized a two-dimensional assembled framework CAM-1{$[Ag_{12}(C_6H_{11}S)_6(CF_3COO)_6(TmPyPB)_2]$. $(C_4H_8O_2)_3$} constructed from an Ag_{12} cluster as SBU interconnected through a tritopic TmPyPB (=1,3,5-Tris(3-pyridyl-3-phenyl)benzene) linker. A pyridine-coordinated Ag_{12} molecular cluster {$[Ag_{12}(C_6H_{11}S)_6(CF_3COO)_6(C_5H_5N)_6]$. $4H_2O$}, abbreviated as NC-

[*] P. Chandrashekar, Prof. S. Mandal
School of Chemistry, Indian Institute of Science Education and Research Thiruvananthapuram
Kerala-695551 (India)
E-mail: sukhendu@iisertvm.ac.in
G. Sardar, Prof. D. Kabra
Department of Physics, Indian Institute of Technology Bombay
Powai, Mumbai, 400076 (India)
Dr. T. Sengupta, Dr. A. C. Reber, Prof. S. N. Khanna
Department of Physics, Virginia Commonwealth University
Richmond, VA-23220 (USA)
E-mail: snkhanna@vcu.edu
Dr. P. K. Mondal
Elettra-Sincrotrone Trieste
S.S. 14 Km 163.5 in Area Science Park, Basovizza, 34149 Trieste (Italy)
Dr. P. Deria
School of Chemical & Biomolecular Science, Southern Illinois University
1245 Lincoln Drive, Carbondale, IL-62901 (USA)
E-mail: pderia@siu.edu

1, was also prepared, and crystallized; NC-1 was used as a benchmark sample to establish the structural correlation to the photophysical properties of the two-dimensional CAM-1 framework. In solid-state, NC-1 represents a supramolecular structure that is built out of non-covalent interaction, whereas the 2D CAM-1 is constructed by interconnecting the cluster nodes through coordination bonds. The variable extent of rigidity imparted by assemblies renders differences in the cluster compression and intra-cluster Ag–Ag distances in the respective cluster units. Analyses of comprehensive temperature-dependent PL studies suggest that the LMMCT-derived cluster-centered PL can be modulated by such assemblies. In particular, the specific arrangement of the Ag_{12} cluster in CAM-1 and NC-1 led to tuning the ΔE_{ST}, which in turn, defines the singlet-triplet (reverse) intersystem crossing rate constant. The TmPyPB-separated cluster assembly in CAM-1 was found to have larger ΔE_{ST} compared to that of NC-1, which required higher temperatures for the reverse populations of the singlet state in CAM-1. This structure-correlated study underscores the avenue to tune the assembly for defining the photophysical properties to develop cluster-based optoelectronic composition operating in ambient temperature.

Results and Discussion

CAM-1 was synthesized through a one-pot method with the addition of Ag-SC_6H_{11} complex, $AgCF_3COO$, and the linker TmPyPB in a mixture of CH_3CN (acetonitrile) and $C_4H_8O_2$ (1,4-dioxane) solvents. CAM-1 $\{[Ag_{12}(C_6H_{11}S)_6(CF_3COO)_6\text{-}(TmPyPB)_2]\ (C_4H_8O_2)_3\}$, (Figures 1 and S1), crystallizes with $P2_1/n$ (14) space group (Table S1). The cluster core of CAM-1 consists of 12 silver atoms arranged in an empty cuboctahedron structure (Figure 1a). It can be visualized in three layers: six silver atoms occupying the hexagonal center of the cuboctahedron and further capped by six silver atoms forming the triangular cupolas at the top and bottom (Figure S2). The primary protecting ligand cyclohexane thiol, bridging the six square faces of the cuboctahedron through a $\mu^4\text{-}\eta^1\text{:}\eta^1\text{:}\eta^1\text{:}\eta^1$ ligation mode, linking four neighbouring silver atoms (Figure 1b). Additionally, six CF_3COO^- auxiliary ligands protect the cluster core. Among these, four CF_3COO^- ligands, each bind to two different silver atoms in $\mu^2\text{-}\eta^2$ mode, while the remaining two CF_3COO^- ligands bind through η^1 mode to one silver atom each (Figure 1c). Each of the six vertices silver of the cuboctahedron is coordinated by the nitrogen atom ($d_{Ag\text{-}N}$ = 2.25 Å) from TmPyPB linker, connecting to six other clusters (Figures 1d and S3). From the other perspective, each TmPyPB linker connects to three clusters, leading to the extension of the structure in two dimensions along the *ab* plane (Figures 1e and S4). The stacked layers are separated by 12.52 Å (Figure S5) and 1, 4-dioxane solvent molecules reside in the void space as depicted in Figure S6. All silver atoms are in the 'closed-shell' +1 oxidation state and are held together by argentophilic interactions[8] with an average Ag(I)–Ag(I) distance of 3.12 Å that is shorter than the sub-van der Waals contacts (ca. 3.44 Å) between the silver atoms. The bond lengths for Ag–S, and Ag–O vary from 2.4 to 2.6 Å and 2.3 to 2.6 Å, respectively.

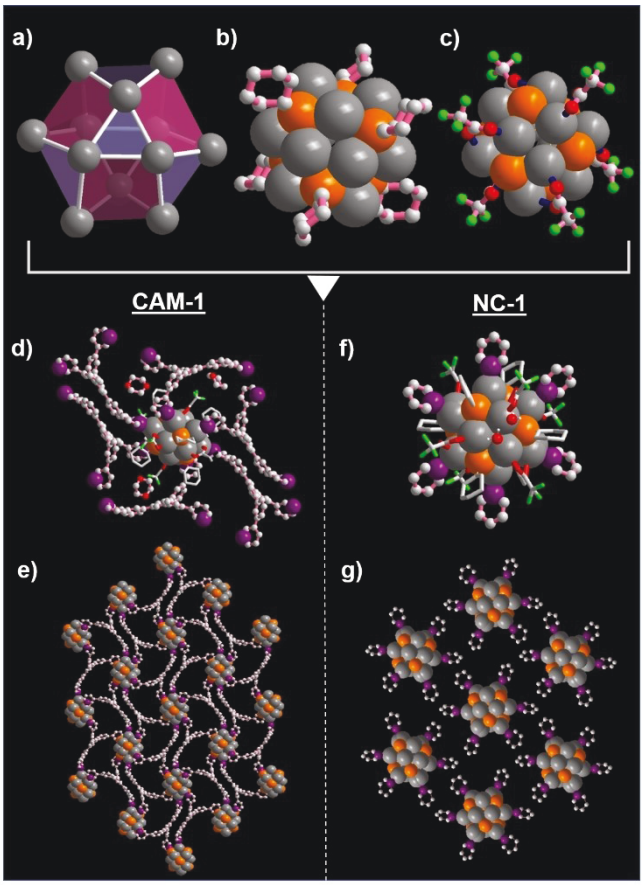

Figure 1. Structural anatomy of CAM-1 and NC-1: (a–c) Representation of Ag_{12} empty cuboctahedron structure protected by cyclohexane thiol and CF_3COO^- ligands, respectively, in CAM-1 and NC-1, (d, f) Nitrogen atom binding to the vertices silver, via the linker TmPyPB in CAM-1 and the pyridine ligand in NC-1, (e, g) Assembly pattern, where CAM-1 forms two-dimensional extended structure by tritopic linker and in NC-1 via the non-covalent interaction by monotopic ligand (observed in the *ab* plane). The color code: Ag-gray, S-orange, O-red, F-bright green, N-violet, C-off-white. All hydrogen atoms are omitted for clarity.

NC-1 was prepared following a similar one-pot synthesis procedure, with the substitution of pyridine instead of TmPyPB in the reaction mixture. The crystal of NC-1, $\{[Ag_{12}(C_6H_{11}S)_6(CF_3COO)_6(C_5H_5N)_6].\ 4H_2O\}$ (Figures S7 and 1f, g), also crystallized with the space group $P2_1/n$ (14) (Table S2). NC-1 has a similar cluster core, with 12 Ag atoms, protected by cyclohexane thiol and CF_3COO^- ligands in a manner analogous to CAM-1 (Figures 1a–c). The average distance between Ag–Ag is 3.16 Å. The bond lengths for Ag–S, and Ag–O vary from 2.4–2.5 Å, and 2.3–2.6 Å, respectively. The pyridine nitrogen atom coordinatively binds to the vertices silver atom of the cuboctahedron, with an average Ag–N distance of 2.26 Å (Figure 1f). Electrospray ionization-mass spectrometry (ESI-MS) analysis of NC-1 shows an intense peak at m/z 2543.9934 in the positive mode matching well with the simulated isotopic pattern of the molecular fragment $\{Ag_{12}(C_6H_{11}S)_3\text{-}$

$(CF_3COO)_8\}^+$ (Figure S8). Overall, both CAM-1 and NC-1 crystallized similarly, differing in their assembly pattern (Figures 1e, g).

The phase purity of the bulk CAM-1 and NC-1 samples was validated by matching their experimental Powder X-ray diffraction (PXRD) patterns with their respective simulated patterns generated from their solved crystal structure (Figures S9 and S10). The Scanning Electron Microscope (SEM) images provided the notion of stacked layer morphology for two-dimensional CAM-1, whereas NC-1 displayed a block-like morphology (Figures S11a, b, and S12a). Additionally, SEM Energy-Dispersive X-ray Spectroscopy (EDS) analysis confirmed the presence of all the elements validating the chemical composition of the samples (Figures S11c and S12b). Analysis of the X-ray Photoelectron Spectroscopic (XPS) data (survey spectrum) confirmed the presence of all the elements, namely Ag, S, N, O, and F. The binding energies of Ag $3d_{5/2}$ and Ag $3d_{3/2}$ were observed at 368.51 and 374.51 eV, respectively for CAM-1, while for NC-1, the values were 368.19 and 374.19 eV, respectively.[9] These findings provide evidence for the presence of silver in the +1 oxidation state in both compounds. Furthermore, the S binding energy approximately at 163 eV, observed for both NC-1 and CAM-1, indicates the involvement of sulfur in bridging the silver atoms[7a] (Figures S13 and S14).

The solid-state absorption spectrum of CAM-1 displays broad bands with low-energy transition appearing at 360 nm (Figure S15). A similar UV/Vis absorption spectral envelope for NC-1 indicates the cluster-centered absorption in both CAM-1 and NC-1 samples (Figure S16). At room temperature (RT), CAM-1 exhibits two emission bands peaking at 440 nm and 575 nm. Excitation spectra probed for the 575 nm peak revealed two prominent excitation bands appearing at 325 nm and 360 nm, whereas the excitation spectra probed for the 440 nm peak only displayed a single band at 325 nm (Figure S17). In contrast, the NC-1 sample displayed emission at 605 nm (accompanied by a weak broad emission at ≈450 nm) with a corresponding excitation band appearing at 360 nm (Figure S18). Based on these data, the low-energy bands in the PL spectra can be assigned to the cluster-derived transitions and the one at higher energy (440 nm) can be attributed to be a coordinated ligand-derived band.[10] The excitation-emission mapping spectra corroborate with this assignment as the higher-energy excitation yielded less population to the cluster-centered excited state (which was selectively obtained by the low-energy excitation; Figure S21).

The intriguing feature of PL has become apparent in temperature-dependent studies. Analyses of the PL spectra of CAM-1 collected over the range of temperatures suggest an unaltered 440 nm high-energy peak that intensified (up to 5x) at low temperature (LT) (Figures 2a, b, and S22). For the low-energy manifold, the shoulder appearing at 660 nm (commonly observed in relevant CAM materials)[5d,6,11] also remains unchanged. The FWHM obtained by deconvoluting the PL spectra for both the 440 nm and 660 nm peaks are distinct, $4850 \pm 155\ cm^{-1}$ and $1550 \pm 150\ cm^{-1}$, respectively (see Figure S23 and Table S3).[12] The 575 nm peak (seen at RT), however, shifted to low-energetic 625 nm at LT which intensified up to 180 times (Figure 2a). Deconvolution of the spectral envelop (see Supporting Information sec 11.1) revealed that the peak shift is associated with the relative intensity of two underlying peaks centered at 578 nm ($1600 \pm 250\ cm^{-1}$) and 620 nm ($1475 \pm 125\ cm^{-1}$) stemming from the different extent of their temperature-dependent populations.

As shown in Figure S22, emission spectra measured at LT are dominated by the 620 nm emission band, which, with the rise in temperature (87–297 K), showed a gradual decrease in its intensity with a concomitant increase in the higher energy 578 nm emission band. Such behavior is reminiscent of RISC from the triplet to the singlet.[13] Analyses through spectral deconvolution suggest that at ≈175 K the radiative population in the two associated excited states were similar, and above this temperature, the 578 nm band dominates (Figure S23). Furthermore, singlet oxygen emission, observed only at LT and not at RT (Figure S24) corroborates this assignment.[14] For non-adiabatic transitions between two states, the rate constant can be expressed as[15]

$$k = \left(2\pi/\hbar\right) V^2 f_{FC} \tag{1}$$

For singlet↔triplet intersystem crossing (ISC), V will be the spin-orbit coupling (SOC) matrix element ($V_{SOC} = \langle \psi_{S_1} | \widehat{H}_{SO} | \psi_{T_1} \rangle$) and f_{FC} is the Franck–Condon factor. Sizable V_{SOC} can be achieved in these Ag-clusters (through the large Z_{eff} [effective nuclear charge] term, defining the heavy atom effect, incorporated within the $\widehat{H}_{SO}$). For such cluster-derived lowest-energy singlet and triplet states, without involving a large structural change (in their equilibrium coordinate) the f_{FC} is defined by the energy-gap law[16] and can be approximately expressed as

$$f_{FC} \approx \frac{1}{\sqrt{4\lambda k_B T}} \exp\left[-\frac{(\Delta E_{ST} + \lambda)^2}{4\lambda k_B T}\right] \tag{2}$$

Where ΔE_{ST} is the energy gap between the S_1 and T_1 states at their equilibrium structure, λ is the reorganization energy (i.e., the difference between the S_1 state energy at the T_1 and S_1 equilibrium geometries).[15,17] It is therefore clear that, within such rigid assemblies, assuming a comparable V_{SOC} and λ, ΔE_{ST} will be the major factor defining the rate of the RISC. While a temperature-dependent emission behavior was observed in certain nanoclusters and their assembled materials,[5b,d,7a–b,13a–c] modulation of their RISC through tuning of their ΔE_{ST} as a function of the assembly was not established. This was mainly due to a large variation in chemical and intra-cluster structure among the assembled materials.

The shift recorded in the temperature-dependent emission profile, suggests a $\Delta E_{ST} \approx 0.14$ eV ($1150\ cm^{-1}$; see Table-S3), which leads to a thermally variable population between two spin states.[18] Therefore, at LT, the triplet-based (phosphorescence) emission ($T_1 \rightarrow S_0$) is dominating and with an increase in temperature, a reverse population of

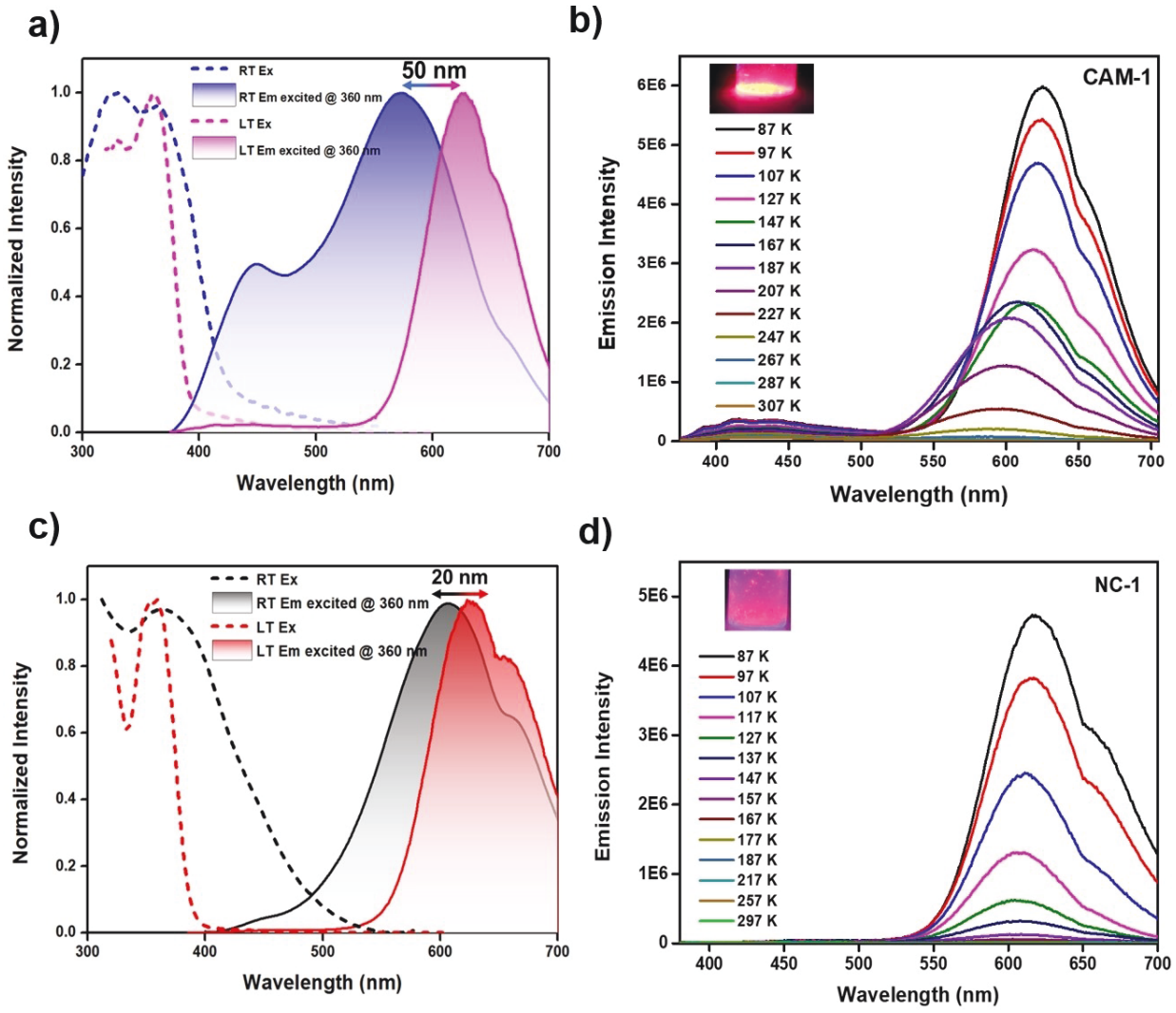

Figure 2. (a) CAM-1, Excitation spectra (blue dotted line) probed for 575 nm emission peak, as well as the emission spectra (blue solid line) upon 360 nm excitation at RT. The excitation spectra (magenta dotted line) probed for 625 nm emission, along with the emission spectra (magenta solid line) obtained under 360 nm excitation at LT. (b) The temperature-dependent emission spectra of CAM-1 in solid state under 360 nm excitation. Inset: photographs of CAM-1 crystals excited by hand-held UV lamp (365 nm) immediately after taking the crystal sample out from liquid nitrogen. (c) NC-1, Excitation spectra (black dotted line) probed for 605 nm emission peak, as well as the emission spectra (black solid line) upon 360 nm excitation at RT. The excitation spectra (red dotted line) probed for 620 nm emission, along with the emission spectra (red solid line) obtained under 360 nm excitation at LT. (d) The temperature-dependent emission spectra of NC-1 in solid state under 360 nm excitation. Inset: photographs of NC-1 crystals excited by a hand-held UV lamp (365 nm) immediately after taking the crystal sample out from liquid nitrogen.

the S_1 state increases in a way that at ≈175 K the S_1 and T_1 populations are comparable, and at a higher temperature, the S_1 population (fluorescence through RISC) dominates. Analyses of the emission decay profiles collected at the emission maxima (Figure S25; Table 1) suggest that at 77 K, a sizable excited-state population radiatively decayed from the triplet state with τ = 73 μs. While the singlet lifetime was fast ≈7 ns, a small proportion (≈10 %) of delayed fluorescence was observed (τ = 93 ns). The profile of these timescales changed with the increase in temperature: the triplet population decreased with a shortened lifetime (≈30 μs), whereas the contribution of the delayed emission doubled. At room temperature, fast emission from the singlet was dominant. From the relative timescales, it is

Table 1: Emission Lifetime Data for CAM-1 and NC-1 powder samples.

Compound	T (K)	λ_{probe} nm	τ_1 ns (%)	τ_2 ns (%)	τ_3 μs (%)
CAM-1	77	640	6.9 (60)	93.5 (10)	73.1 (30)
	187	620	5.0 (68)	80.0 (20)	30.0 (12)
	300	590	1.5 (90)	14.8 (10)	--
NC-1	77	680	≲1 (99)	6.2 (1)	
	180	680	≲1 (99)	4.9 (1)	

Data collected under vacuum; IRF ≈ 1 ns; maximum error manifested in time constants ca ±10 % of the value.

evident that an efficient k_{RISC} and k_{em} overwhelmed the sluggish $T_1 \rightarrow S_0$ recombination process.

A similar temperature-dependent emission study for NC-1 (Figures 2c, d and see Supporting Information sec 12) suggests triplet emission from 610 nm and fluorescence from 590 nm leading to a relatively smaller $\Delta E_{ST} = 0.06$ eV (545 cm^{-1}) compared to the CAM-1 (Figure S26 and Table S4). Such a small gap led to an efficient RISC and, therefore, it took a much lower temperature ($\approx$115 K) for an equal triplet and singlet (repopulated by RISC) population for NC-1 relative to 175 K for CAM-1. Note here that the NC-1 manifests a small ΔE_{ST}, mostly by virtue of its lower S_1 energy therefore a small $\Delta E_{S1\text{-}S0}$ has also led to an efficient nonradiative internal conversion (or intra-system crossing efficiency): the emission for NC-1 was much weak compared to CAM-1, which can be associated with the molecular nonrigidity. The PL decay profile also suggests that the majority of the emission for NC-1 was fast (within the realm of our IRF) (Table 1; Figure S27). A linear plot of emission intensity as a function of pump fluence with slope $\approx$1 suggested that no bi-excitonic triplet-triplet annihilation (TTA) process is involved in repopulating the singlet excited state (Figure S29).[19]

Time-dependent density functional theory (TDDFT) based computation was performed on a cluster model fragment for the NC-1 structure (see Supporting Information Figure S30 for optimized ground-state cluster model geometry). This computation result suggests that a weak lowest energy HOMO–LUMO derived vertical transitions at $\approx$560 nm, where the higher energy broad absorption envelope is contributed by many closely spaced (energetically) transitions (see Supporting Information sec 14.2); among these, an intense 350 nm transition appears to be stemming from delocalized molecular orbitals (MOs) to three superatomic P orbitals, whereas the 403 nm transition is primarily due to the optical transition from a delocalized MO to the superatomic S orbital of the core cluster (Figure S32). The same conclusion can be drawn from the natural transition orbital (NTO) analysis which is included in Figure S33. These transitions can be ascribed to LMMCT transition (S $\rightarrow$Ag) mixed with the metal-centered (ds/dp) state.[6] TDDFT computation also evinced a $\Delta E_{ST} \approx 0.07$ eV which matches reasonably well with the experimental data (Figure 3 and Table S5).

To evaluate the electronic properties of the NC-1 and CAM-1 crystalline solids, density of state (DOS), and band structures were computed on the respective optimized structures (Figure S36). The result (Figure S37) suggests a larger (2.32 eV) band gap for CAM-1 than the NC-1 (2.23 eV). This relative trend tracks with the difference in band gap energies observed experimentally (i.e., 2.15 and 2.04 eV, respectively, measured from their emission peak). The corresponding theoretical optical absorption spectra (Figure S38) for both structures also show a close resemblance with the experimental data (see earlier sec 8.1). The projected DOS diagram reveals that the composition of valence band maximum (VBM) and conduction band minimum (CBM) are similar for both structures. The band

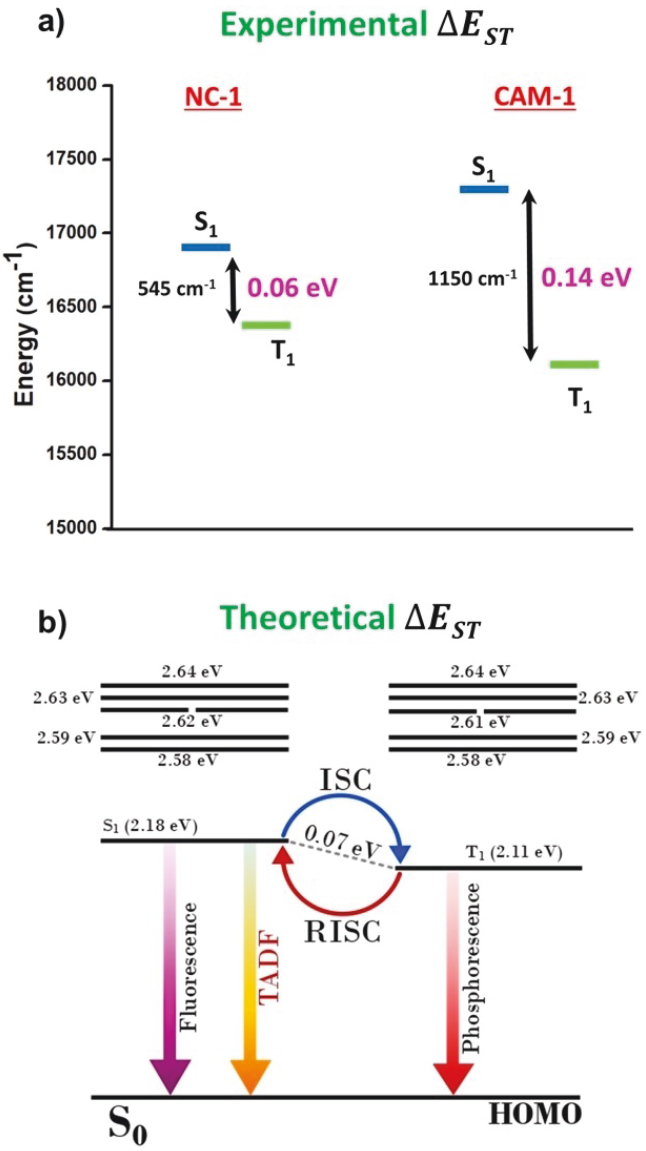

Figure 3. (a) Experimental $\Delta E_{S1\text{-}T1}$ of CAM-1 (right), NC-1 (left). (b) TDDFT computed excited state energy levels highlighting $\Delta E_{S1\text{-}T1}$ in an NC-1 model (defined by a single cluster; see Supporting Information sec 13).

diagrams are also similar and mostly composed of discrete lines (see Supporting Information sec 14.3).

While a shorter Ag–Ag distance commonly leads to a red-shifted emission,[20] CAM-1 (with $\approx$0.04 Å shorter intra-cluster nearest Ag–Ag distance than that in NC-1; Figure S39) entailed a blue-shifted transition compared to NC-1. The structural feature underscores a striking difference in the extent of the cluster packing of these two assemblies (Figure 4).[21] In CAM-1, a relatively rigid framework construct is achieved by the interconnected assembly through the TmPyPB coordination linkage. A compressed cluster–defined by a *ca* 0.13 Å shorter opposite Ag–Ag distance in CAM-1 (Figure S40 and Table S6) appears to define the electronic properties of the clusters.[20c] A shorter

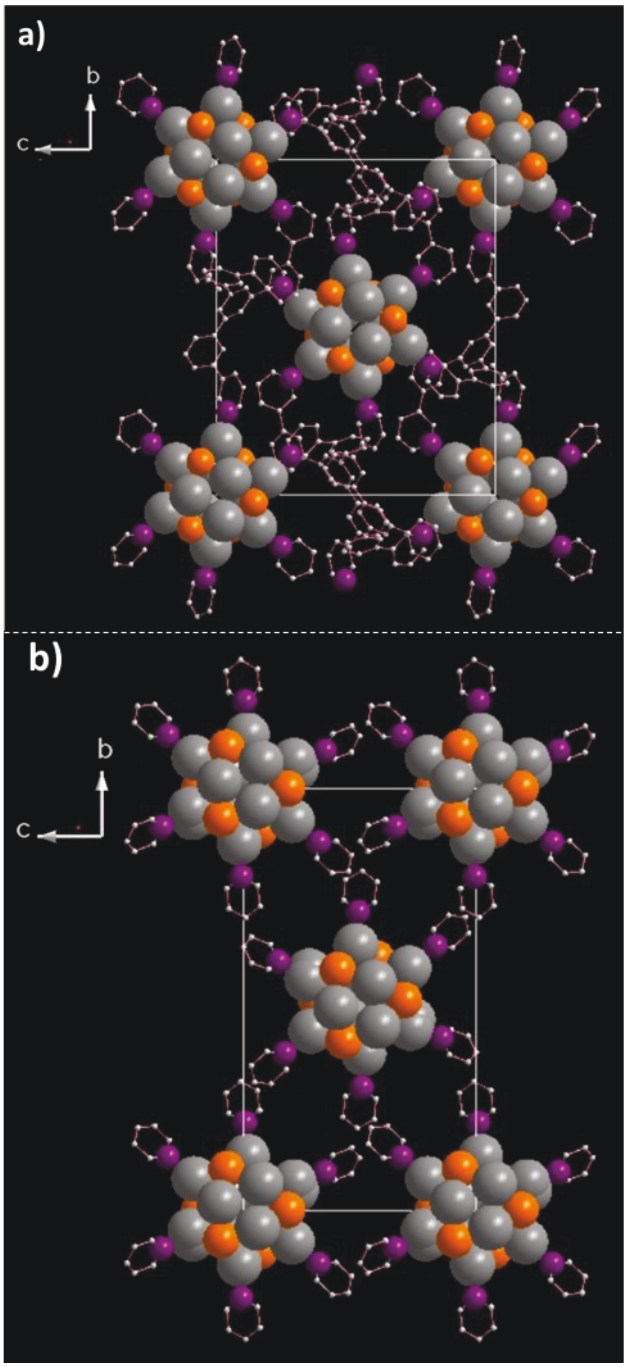

Figure 4. Cluster assembly in the crystal lattice via; (a) coordination assembly in CAM-1, (b) non-covalent interaction in NC-1 (viewed along *a* direction). Color code: Ag-gray, S-orange, N-violet, C-off white. For clarity, all O, F, and H atoms are omitted.

nearest Ag–Ag distance and an overall compressed cluster entailed their ΔE_{ST} in CAM-1 relative to NC-1.

Analysis of the steady-state emission profiles provides the relative contribution of the respective singlet and triplet emissions at a given probe temperature, which can be expressed in terms of equilibrium constants between S_1 and T_1 states at various temperatures.[22] A van't Hoff plot of the ln(K) vs. 1/T data using the expression

$$\ln K = \frac{\Delta S}{R} - \frac{\Delta H}{RT}$$

provides a slope (see Supporting Information sec 16) from which ΔH value of 190.7 cm^{-1} for CAM-1 and 106 cm^{-1} for NC-1 can be obtained. The extent of difference in ΔH is similar to that observed for the trend in ΔE_{ST} (Figure S45). Given that for the solid system, ΔH defines the change in internal energy, we can infer that the extent of S_1-T_1 population difference in two cluster assemblies is majorly tied to their difference in the internal energy differences stemming from their small structural difference (see above).

Conclusion

We probe the photophysical behavior as a function of difference in the assemblies of Ag_{12} nanoclusters. For that, two systems were built through varying ligands; introduced via Ag–N bonds from the TmPyPB linker in CAM-1 and through inter-cluster interactions (non-covalent) in NC-1 using monotopic pyridine. Detailed examination of their PL properties revealed a temperature-dependent emission behavior that differed by their respective structures. Defined by a small energy gap (ΔE_{ST}), temperature-dependent population shifts towards the higher energy S_1 state, through a RISC of the T_1 state was observed. Notably, the rigid compressed core in CAM-1, with Ag_{12} cluster distanced by the tritopic linker, requires a higher temperature (175 K) for RISC compared to NC-1 (115 K). Such differences in cluster packing induced by the coordinate assembly played a crucial role in defining intra-cluster electronic interactions and Ag–Ag length scales, which has resulted in a difference in ΔE_{ST}: for CAM-1, higher S_1 energy and lower T_1 energy resulted in a larger S_1–T_1 gap (ΔE_{ST} = 0.14 eV), whereas NC-1 has a smaller gap (ΔE_{ST} = 0.06 eV). We believe, these findings underscore the significance of nanocluster arrangements in supramolecular chemistry, which provides a synthetic toolkit for designing cluster assembly with tailored photophysical properties for their utilities in various optoelectronic schemes.

Supporting Information

Details on synthesis, crystallographic information, optical images, crystal structure details, ESI-MS, PXRD, SEM, XPS, solid-state UV/Vis spectra, excitation and emission spectra, temperature-dependent emission studies, TRPL spectra, singlet oxygen emission spectra, theoretical details, and references.

Accession codes. Deposition Number 2293356 (CAM-1), 2293355 (NC-1), contain(s) the supplementary crystallographic data for this paper. These data are provided free of charge by the joint Cambridge Crystallographic Data Centre and Fachinformationszentrum Karlsruhe Access Structures service.

Acknowledgements

PC acknowledges the Council of Scientific & Industrial Research India for fellowship. The authors acknowledge Mr. Akashdeep Nath for assisting on TDDFT of the linker molecule. The authors thank Ms. Devika Rajan and Mr. Gokul Krishnan for helping during the material synthesis. The authors wish to extend their gratitude to Ms. Saniya Gratious for her valuable assistance in conducting the ESI-MS analysis. The authors are thankful to Dr. Noohul Alam for his assistance in the graphical illustration. PD acknowledges NSF CAREER CHE-1944903.

Conflict of Interest

The authors declare no conflict of interest.

Data Availability Statement

The data that support the findings of this study are available from the corresponding author upon reasonable request.

Keywords: Cluster Assembled Material · Nanocluster · Phosphorescence · Silver Cluster · Thermally Activated Fluorescence

[1] S. A. Claridge, A. W. Castleman, S. N. Khanna, C. B. Murray, A. Sen, P. S. Weiss, *ACS Nano* **2009**, *3*, 244–255.
[2] X. Kang, M. Zhu, *Coord. Chem. Rev.* **2019**, *394*, 1–38.
[3] S. Bonacchi, S. Antonello, T. Dainese, F. Maran, *Chem. Eur. J.* **2021**, *27*, 30–38.
[4] a) A. Ebina, S. Hossain, H. Horihata, S. Ozaki, S. Kato, T. Kawawaki, Y. Negishi, *Nanomaterials* **2020**, *10*, 1105; b) R. Jin, C. Zeng, M. Zhou, Y. Chen, *Chem. Rev.* **2016**, *116*, 10346–10413; c) X. Kang, M. Zhu, *Chem. Soc. Rev.* **2019**, *48*, 2422–2457; d) T. Chen, H. Lin, Y. Cao, Q. Yao, J. Xie, *Adv. Mater.* **2022**, *34*, 2103918.
[5] a) Y. Jin, C. Zhang, X. Y. Dong, S. Q. Zang, T. C. W. Mak, *Chem. Soc. Rev.* **2021**, *50*, 2297–2319; b) Z. Y. Wang, M. Q. Wang, Y. L. Li, P. Luo, T. T. Jia, R. W. Huang, S. Q. Zang, T. C. W. Mak, *J. Am. Chem. Soc.* **2018**, *140*, 1069–1076; c) R. W. Huang, Y. S. Wei, X. Y. Dong, X. H. Wu, C. X. Du, S. Q. Zang, T. C. W. Mak, *Nat. Chem.* **2017**, *9*, 689–697; d) M. J. Alhilaly, R. W. Huang, R. Naphade, B. Alamer, M. N. Hedhili, A. H. Emwas, P. Maity, J. Yin, A. Shkurenko, O. F. Mohammed, M. Eddaoudi, O. M. Bakr, *J. Am. Chem. Soc.* **2019**, *141*, 9585–9592; e) W. A. Dar, A. Jana, K. S. Sugi, G. Paramasivam, M. Bodiuzzaman, E. Khatun, A. Som, A. Mahendranath, A. Chakraborty, T. Pradeep, *Chem. Mater.* **2022**, *34*, 4703–4711.
[6] R. Huang, X. Dong, B. Yan, X. Du, D. Wei, S. Zang, T. C. W. Mak, *Angew. Chem. Int. Ed.* **2018**, *157*, 8560–8566.
[7] a) Q. Q. Xu, X. Y. Dong, R. W. Huang, B. Li, S. Q. Zang, T. C. W. Mak, *Nanoscale* **2015**, *7*, 1650–1654; b) B. Li, R.-W. Huang, J.-H. Qin, S.-Q. Zang, G.-G. Gao, H.-W. Hou, T. C. W. Mak, *Chem. Eur. J.* **2014**, *20*, 12416–12420; c) Y. L. Li, W. M. Zhang, J. Wang, Y. Tian, Z. Y. Wang, C. X. Du, S. Q. Zang, T. C. W. Mak, *Dalton Trans.* **2018**, *47*, 14884–14888.
[8] H. Schmidbaur, A. Schier, *Angew. Chem. Int. Ed.* **2015**, *54*, 746–784.
[9] The Ag binding energies for CAM are 0.32 eV larger than that in in NC-1; this could be due to shorter Ag–Ag distance in CAM-1.
[10] Corresponding TDDFT computation for the TmPyPB showed n→π* at 246 nm for the free linker and π→π* transitions appearing at 282 nm for the two closely spaced linker in CAM-1, where experimental spectra of linker show 350 nm emission at 290 nm excitation and 440 nm emission at 325 nm excitation in CAM-1 (Sec 9, Figures S19 and S20).
[11] J. Y. Wang, R. W. Huang, Z. Wei, X. J. Xi, X. Y. Dong, S. Q. Zang, *Chem. Eur. J.* **2019**, *25*, 3376–3381.
[12] The large difference in their spectral linewidth is also suggestive of different origin as assigned above.
[13] a) Z. R. Yuan, Z. Wang, B. L. Han, C. K. Zhang, S. S. Zhang, Z. Y. Zhu, J. H. Yu, T. D. Li, Y. Z. Li, C. H. Tung, D. Sun, *Angew. Chem. Int. Ed.* **2022**, *61*, e202211628; b) Z. Han, X. Y. Dong, P. Luo, S. Li, Z. Y. Wang, S. Q. Zang, T. C. W. Mak, *Sci. Adv.* **2020**, *6*, eaay0107; c) L. Luo, Z. Liu, X. Du, R. Jin, *Commun. Chem.* **2023**, *6*, 6–11; d) Z. Liu, M. Zhou, L. Luo, Y. Wang, E. Kahng, R. Jin, *J. Am. Chem. Soc.* **2023**, *145*, 19969–19981.
[14] a) C. Zhu, J. Xin, J. Li, H. Li, X. Kang, Y. Pei, M. Zhu, *Angew. Chem. Int. Ed.* **2022**, *61*, e202205947; b) Y. Song, Y. Li, M. Zhou, X. Liu, H. Li, H. Wang, Y. Shen, M. Zhu, R. Jin, *Sci. Adv.* **2021**, *7*, eabd2091.
[15] C. M. Marian, *Annu. Rev. Phys. Chem.* **2021**, *72*, 617–640.
[16] R. Englman, *Mol. Phys.* **1970**, *18*, 145–164.
[17] a) Y. Olivier, B. Yurash, L. Muccioli, G. D'Avino, O. Mikhnenko, J. C. Sancho-García, C. Adachi, T. Q. Nguyen, D. Beljonne, *Phys. Rev. Mater.* **2017**, *1*, 075602; b) P. K. Samanta, D. Kim, V. Coropceanu, J. L. Brédas, *J. Am. Chem. Soc.* **2017**, *139*, 4042–4051.
[18] M. Beliaeva, A. Belyaev, E. V. Grachova, A. Steffen, I. O. Koshevoy, *J. Am. Chem. Soc.* **2021**, *143*, 15045–15055.
[19] a) F. B. Dias, K. N. Bourdakos, V. Jankus, K. C. Moss, K. T. Kamtekar, V. Bhalla, J. Santos, M. R. Bryce, A. P. Monkman, *Adv. Mater.* **2013**, *25*, 3707–3714; b) A. Dey, A. Rao, D. Kabra, *Adv. Opt. Mater.* **2017**, *5*, 1600678.
[20] a) X. P. Wang, T. P. Hu, D. Sun, *CrystEngComm* **2015**, *17*, 3393–3417; b) Z. H. Yan, X. Y. Li, L. W. Liu, S. Q. Yu, X. P. Wang, D. Sun, *Inorg. Chem.* **2016**, *55*, 1096–1101; c) Y. M. Su, Z. Z. Cao, L. Feng, Q. W. Xue, C. H. Tung, Z. Y. Gao, D. Sun, *Small* **2022**, *18*, 2104524; d) V. W. W. Yam, K. K. W. Lo, *Chem. Soc. Rev.* **1999**, *28*, 323–334.
[21] In solid state, cluster nodes are arranged in BCC type of lattice (Figure S41) and the shortest distance between two pyridine ring in the crystal packing is given in Figure S42.
[22] Assuming that a comparable fraction of the total population from a given state (S_1 or T_1) radiatively decays.

Manuscript received: November 14, 2023
Accepted manuscript online: December 11, 2023
Version of record online: ■■, ■■

Research Articles

Nanoclusters

P. Chandrashekar, G. Sardar, T. Sengupta, A. C. Reber, P. K. Mondal, D. Kabra, S. N. Khanna,* P. Deria,* S. Mandal* _____ **e202317345**

Modulation of Singlet-Triplet Gap in Atomically Precise Silver Cluster-Assembled Material

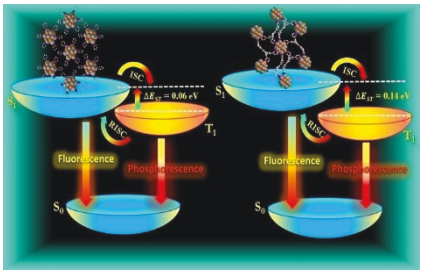

The singlet-triplet energy gap was modulated by controlling the inter-cluster interaction defined by the supramolecular arrangements of Ag_{12} nanoclusters.